Nanoscale

The effect of localized surface plasmon resonance on the emission color change in organic light emitting diodes†

Illhwan Lee,‡[a] Jae Yong Park,‡[a] Kihyon Hong,[a] Jun Ho Son,[b] Sungjun Kim[a] and Jong-Lam Lee*[a]

Three primary colors, cyan, yellow, and green, are obtained from Ag nano-dot embedded organic light emitting diodes (OLEDs) by localized surface plasmon resonance (LSPR). By changing the thickness of the Ag film, the size and spacing of Ag nano-dots are controlled. The generated light from the emissive layer in the OLEDs interacts with the free electrons near the surface of the Ag nano-dots, which leads to LSPR absorption and scattering. The UV-visible absorption spectra of glass/ITO/Ag nano-dot samples show intense peaks from 430 nm to 520 nm with an increase of Ag nano-dot size. And also, the Rayleigh scattering spectra results show the plasmon resonance wavelength in the range of 470–550 nm. The effect of the LSPR of Ag nano-dots on the change of emission color in OLEDs is demonstrated using 2 dimensional finite-difference time-domain simulations. The intensity of the electro-magnetic field in the sample with 5 nm-thick Ag is low at the incident wavelength of 500 nm, but it increases with the incident wavelength. This provides evidence that the emission color change in OLEDs originates from LSPR at the Ag nano-dots. As a result, the emission peak wavelength of OLEDs shifted toward longer wavelengths, from cyan to yellow-green, with the increase of Ag nano-dot size.

1. Introduction

Organic light-emitting diodes (OLEDs) have potential applications such as full color flat panel displays, flexible display devices, and solid-state lighting.[1–5] However, normal OLEDs emit only a single color, which is determined by the organic materials of the emissive layer. For various applications, OLEDs with tunable emission color are desirable. Color-tunable OLEDs have been fabricated by many strategies,

including doping of the emissive layer,[6] the use of exterior color tuning layers,[7,8] and the use of interior complex layers,[9] but these methods have limitations such as degradation of electroluminescence properties, complex processing techniques, and high cost.

Localized surface plasmon resonance (LSPR) is a possible method to produce color-tunable OLEDs. LSPR results from the coupling between the incident light and the free electron gas at the surface of a nano-sized metal object.[10,11] Light is an electromagnetic (EM) wave, acting as an oscillation of free electron gases of metals.[12] These oscillations occur at specific frequencies for each kind of metal. The basic phenomenon is surface plasmon resonance (SPR), which is non-radiative because its momentum is higher than the visible-wavelength photon's momentum through free space.[13] However, on rough surfaces, *e.g.* surface textured structures, metal nano-dots, nano-wires, and nano-pyramids,[14–16] the surface roughness reduces the momentum of SPR to less than that of a photon,[13] so coupling between the photons causes some to be absorbed and some to be scattered; this is LSPR.[17–19] There are a number of approaches reported in the literature for using LSPR, which can be categorized into two kinds of groups: optical detection and its enhancement. The optical detector such as surface-enhanced Raman scattering (SERS) is using excitations of metal particles for detection of molecules.[20,21] Also, LSPR is used to enhance the performance of solar cells.[22,23] These studies have been conducted on absorption of photons *via* LSPR. No studies have been reported on the effect of LSPR on the change of color in OLEDs.

In this work, we demonstrate a novel way of tuning the emission color of an OLED by embedding Ag nano-dots between the anode and organic materials of the OLED. Color tuning is related to LSPR absorption and scattering. Some photons that are emitted at the active layer simulate collective oscillations with electrons in metals. Thus, controlling the wavelength of LSPR absorption and scattering could lead to the tuning of the emission wavelength of an OLED. The wavelength of LSPR absorption and scattering could be changed by controlling the size and spacing of Ag nano-dots. Photons with

[a]*Department of Material Science and Engineering, POSTECH, Hyojadong, Namgu San 31, Pohang, Kyungbuk, Republic of Korea. E-mail: jllee@postech.ac.kr*
[b]*Department of Bioengineering, UC Berkeley, 442 Stanley Hall, Berkeley, California, USA*
†Electronic supplementary information (ESI) available. See DOI: 10.1039/c5nr07438j
‡These authors contributed equally to this work as first authors.
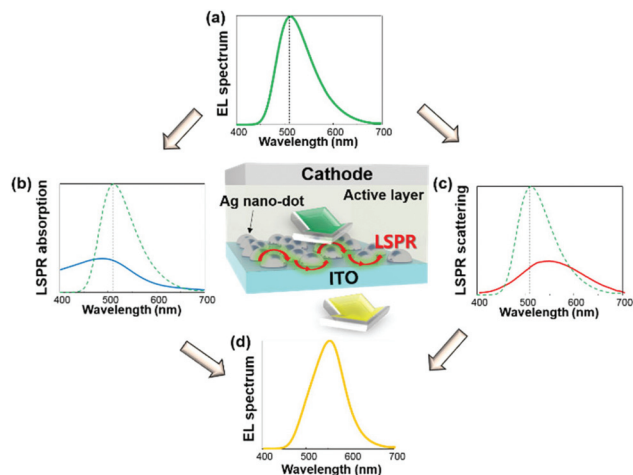
Fig. 1 Schematic explanation of the mechanism for tuning the emission color of OLEDs. (a) Generated emission spectrum from the active layer, (b) LSPR absorption, (c) LSPR scattering, and (d) emission spectrum obtained from pass-through Ag nano-dots.

Table 1 Size of Ag nano-dots and their spacing as a function of Ag thickness

Ag thickness [nm]	Spacing (S_{ND}) [nm]	Avg. dot size (D_{ND}) [nm]
1	20.8	22.7
3	19.8	23.8
5	21.9	31.7
7	33.4	48.1
10	59.9	77.7

wavelengths $\lambda < 514$ nm (the peak center of a normal OLED's emission spectrum, Fig. 1a) were mostly absorbed (Fig. 1b), and those with $\lambda > 514$ nm were scattered (Fig. 1c), as a result the emission spectrum of the OLED was red-shifted (Fig. 1d). Using LSPR, the emission color can be tuned from cyan to yellow-green.

2. Experimental

2.1. Measurement of optical properties

The optical transmittance of an Ag nano-dot was measured at wavelengths of 350–750 nm by UV/Vis spectroscopy (Lambda 750S; Perkin Elmer). The scattering images and spectra of the Ag nano-dot samples were acquired using a dark-field microscopy system with a true color imaging charge-coupled device (CCD) camera and a spectrometer. The UV-Vis absorbance was measured by using a spectrometer. Digital instrument atomic force microscopy (AFM; Digital instruments) was used to observe the surface morphology of the ITO/Ag nano-dot samples. We determined the average value of the nano-dot diameter, D_{ND}, and the spacing, S_{ND}, using an image analysis program (Leopard 2009, Inc. Zootos).

2.2. Device fabrication

To understand the effect of Ag nano-dots on OLED properties, bottom-emitting OLEDs were fabricated. ITO-coated glass (ITO thickness = 170 nm) was used as the substrate. The surface of the ITO-coated glass was cleaned with acetone, iso-propyl alcohol and deionized water in sequence, then dried with high-purity N_2 gas. To produce Ag nano-dots, thin Ag films (0, 1, 3, 5, 7, 10 nm) were deposited on the substrate using a thermal evaporator. The films were grown at 1 Å s^{-1} at a base pressure of $\sim 10^{-6}$ Torr. Then, the samples were annealed by rapid thermal annealing at 300 °C under vacuum (Fig. 1b).

Then 4,4′-bis[N-(1-naphthyl)-N-phenylamino]biphenyl (α-NPD, 70 nm), tris (8-hydroxyquinoline) aluminum (Alq$_3$, 60 nm), LiF (1 nm), and Al (100 nm) were deposited as the hole transport layer (HTL), emissive layer (EML), electron injection layer (EIL), and reflective cathode in sequence. The current density–voltage (J–V) characteristics and luminance L of the devices were measured using an HP-4156A semiconductor parameter analyzer in ambient N_2. Electroluminescence (EL) was measured using a spectrometer.

2.3. Simulation

The 2 dimensional (2D) finite-difference time-domain (FDTD) method with a PML was employed for numerical analysis of the electric field distribution and EL spectrum. The simulation tool is an electromagnetic calculation module (Fullwave) from commercial software Rsoft 2014. 09 (Synopsys and Rsoft Design Group, Inc.). The simulation structure consists of an aluminum cathode 100 nm, LiF (refractive index (n) = 1.39) 1 nm, Alq$_3$ (n = 1.71) 60 nm, NPB (n = 1.82) 70 nm, Ag (n = 0.13) nano-dots, and ITO (n = 2.03) glass. The D_{ND} and S_{ND} are shown in Table 1. The pulse excitation is used for the wavelength response of the designed structure. The discrete Fourier transform (DFT) monitor was used to get cross-sectional spatial electric field distribution. The electric field was obtained in the steady state. The output power intensity as a function of wavelength was used to approximate the EL spectrum of the devices.
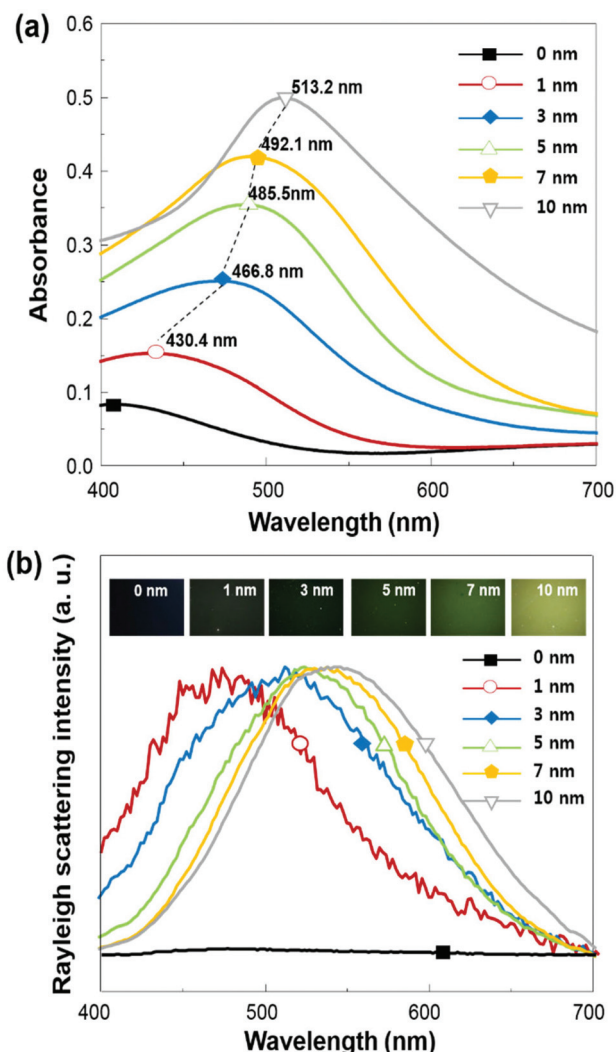
3. Results and discussion

Ag nano-dots can be produced by thermally annealing the Ag film, and their size and spacing can be effectively controlled by changing the initial thickness T_{Ag} of the film. Thermal annealing of the film with T_{Ag} = 0, 1, 3, 5, 7, or 10 nm at 300 °C for 1 min converted them to nano-size dots (Fig. 2a). Both the nano-dot's size and spacing increased with the Ag thickness. As the initial T_{Ag} increased from 1 nm to 10 nm, the D_{ND} increased from 22.7 nm to 77.7 nm, and the S_{ND} between the nano-dots increased from 20.8 nm to 59.9 nm (Fig. 2b and Fig. S1†). Changes in the nano-dot's size and spacing caused color change (Fig. 2c). This could be due to the interaction of light with electrons and the nano-dots, LSPR.

To investigate the occurrence of LSPR at the periphery of the Ag nano-dots, we conducted UV-Vis absorption spectroscopy and Rayleigh scattering spectra measurements of glass/
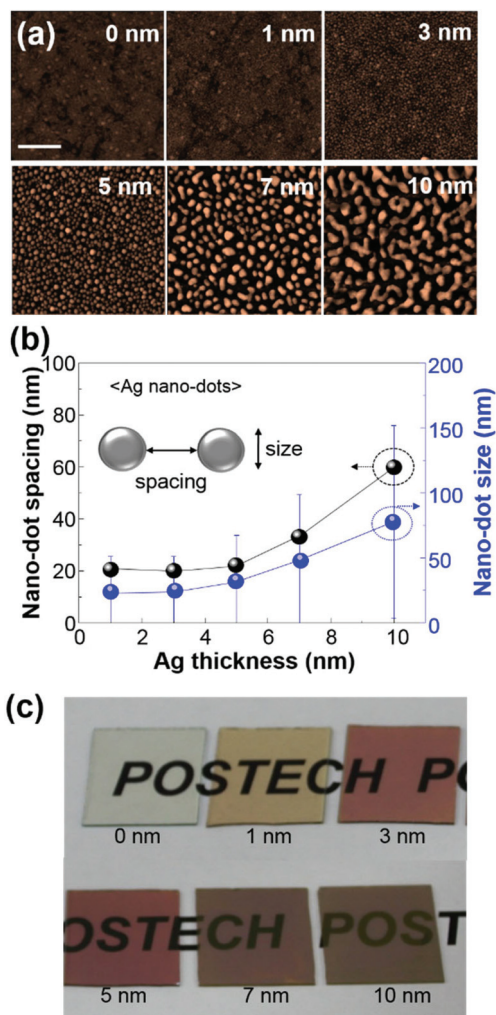
Fig. 2 (a) AFM images of glass/ITO/Ag nano-dot samples. All images are 2μm × 2μm scans (scale bar: 500 nm). (b) Ag nano-dot size D_{ND} (blue line) and spacing S_{ND} (black line) on glass/ITO vs. initial Ag thickness (c) photograph of glass/ITO/Ag nano-dot samples.

Fig. 3 (a) UV-Vis net absorption spectra of glass/ITO/Ag nano-dot samples as a function of Ag thickness. (b) Dark-field reflectance images of glass/ITO/Ag nano-dot samples (inset) and Rayleigh scattering spectra of Ag nano-dot samples at different initial Ag film thicknesses.

ITO and glass/ITO/Ag nano-dot samples (Fig. 3). The glass/ITO sample ($T_{Ag} = 0$ nm) showed an absorption spectrum with a low intensity in the visible region, but the glass/ITO/Ag nano-dots showed a distinct peak centered between $430.4 \leq \lambda \leq 513.2$ nm (Fig. 3a), and its peak wavelength changes with the Ag thickness, that is, the nano-dot's size and spacing as given in Table 1. The absorbance peak intensity increased with the Ag thickness. From the point of view of the symmetry of spectra, the absorbance spectrum was asymmetric at $450 \leq \lambda \leq 650$ nm and dominant at the left shoulder when the Ag thickness is thinner than 7 nm ($1 \leq T_{Ag} \leq 7$ nm). This provides evidence that absorption mainly occurred at a wavelength smaller than $\lambda \leq 514$ nm, relating to the LSPR absorption. At $T_{Ag} = 10$ nm, the absorbance spectrum becomes symmetric at $450 \leq \lambda \leq 650$ nm. The presence of Ag nano-dots affected the dark-field reflectance spectra of the samples. The glass/ITO sample showed no scattering profile (Fig. 3b), but the image brightened as T_{Ag} increased. Such brightening with the increase of

Ag thickness could be due to the LSPR scattering, which induced light scattering over the whole film surface. As the Ag nano-dot size increased, the LSPR scattering wavelength red-shifted from 470 nm to 550 nm. Therefore, tuning the color of OLEDs could be achieved by controlling the size and spacing of nano-dots.

Fig. 4a shows the current density–voltage characteristics of bottom-emitting OLEDs with Ag nano-dots for different Ag thicknesses. The operation voltage of the device without Ag nano-dots was $15.9V$ at a current density of 100 mA cm^{-2}. It changed to $14.1V$ ($T_{Ag} = 1$ nm)–$12.4V$ ($T_{Ag} = 10$ nm) when the Ag nano-dots were inserted. The operation voltage of the Ag nano-dot embedded OLEDs increased at a constant current density because the electric field strengthened due to partial reduction of the organic layer thickness around the inclined region between the peak and valley of the nano-dot structure.[24]
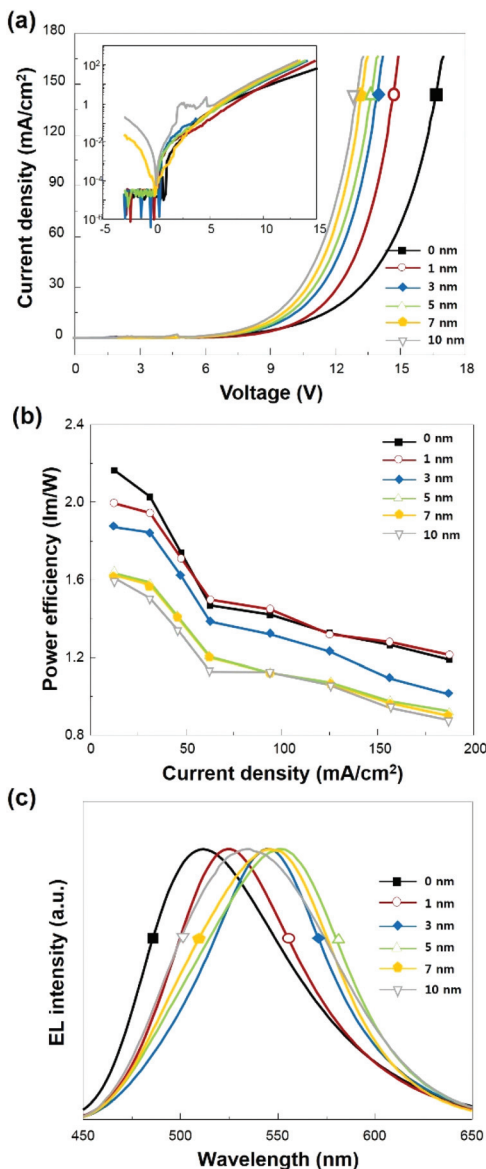
Fig. 4 (a) Current density–voltage characteristics of OLEDs with embedded Ag nano-dots, and leakage current density (inset) (b) current density-power efficiency characteristics of OLEDs with embedded Ag nano-dots (c) EL spectra of OLEDs with Ag nano-dots.

than that with the Ag nano-dots. The power efficiency at 50 mA cm^{-2} was calculated to be 1.74 lm W^{-1} without Ag nano-dots, but it decreased to 1.38 lm W^{-1} with Ag nano-dots (T_{Ag} = 5 nm). Nevertheless, the power efficiency in the Ag nano-dot embedded device was measured to be 79% (T_{Ag} = 5 nm) in comparison with the glass/ITO one (Fig. 4b). Fig. 4c shows the normalized EL spectra of the devices with different Ag thicknesses as a function of wavelength at 62.5 mA cm^{-2}. As T_{Ag} increased, the EL spectra shifted towards high wavelengths. The peak center of the OLED's EL spectrum increases from 514 (cyan) to 552 (yellow-green) nm as T_{Ag} increased from 0 to 5 nm.

We employed 2D FDTD simulations to explain the effect of the LSPR of Ag nano-dots on the change of the emission color in OLEDs. Fig. 5a shows the schematic of the Ag nano-dot embedded OLED structure used in the FDTD calculation composed of a 60 nm-thick Alq$_3$ active layer, a 70 nm-thick NPB layer and a 170 nm-thick ITO electrode. Two kinds of structures, without Ag nano-dots (T_{Ag} = 0 nm, Fig. 5b) and with Ag nano-dots (T_{Ag} = 5 nm, Fig. 5c), on the ITO electrode were simulated. The plane wave emitting from the bottom of the active layer (Alq$_3$) has an excitation spectrum of the Gaussian
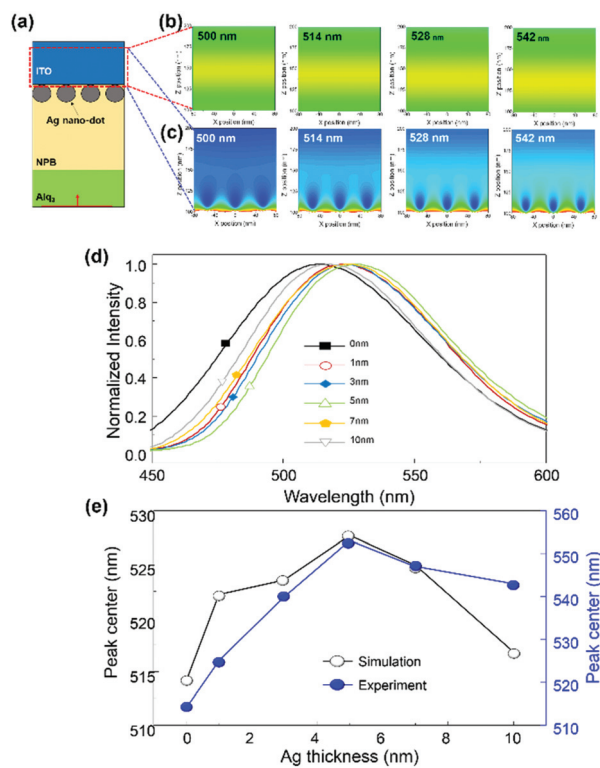

Fig. 5 (a) Schematic illustration of the calculated OLEDs structure with embedded Ag nano-dots. Cross-sectional electric field distribution of the enlarge view of the red dotted box area is shown in (b) 0 nm-thick Ag structure (no Ag nano-dot) and (c) 5 nm-thick Ag nano-dot structure. The electric field is calculated 500, 514, 528 and 542 nm wavelengths. (d) The normalized output power spectra as a function of Ag thickness. (e) Peak center of the output power spectra (simulation: black, experiment: blue).

However, as the 7 and 10 nm-thick Ag were inserted, the leakage current density at −3V increased from 1.8 μA cm^{-2} (T_{Ag} = 0 nm) to 0.02–0.2 mA cm^{-2} (T_{Ag} = 7–10 nm). This large leakage current originated from the roughened surface induced by the Ag nano-dots. Current density–luminance characteristics were measured (Fig. S2a†). The glass/ITO device (T_{Ag} = 0 nm) showed L = 11 000 cd m^{-2} (at 190 mA cm^{-2}). However, the luminance of the Ag nano-dot embedded device (T_{Ag} = 5 nm) decreased to 7000 cd m^{-2}. The decrease of luminance can be explained by the effect of light absorption at the Ag nano-dot interface (Fig. 3a). The plots of power efficiency *versus* current density for the devices are shown in Fig. 4b. OLEDs without Ag nano-dots have higher power efficiency

distribution with the peak center (λ = 514 nm) and FWHM (86 nm), consistent with the experimentally measured EL spectrum in Fig. 4c of the manuscript. Boundary conditions for the FDTD simulation are set to be a perfect matched layer (PML) to avoid the reflected EM wave at the edge of the structure. A cross-sectional discrete Fourier transform (DFT) monitor was used to obtain the spatial electric field distribution. The box marked with a dotted line in red color in Fig. 5a is magnified and given in Fig. 5b for the sample without Ag nano-dots and in Fig. 5c for that with Ag nano-dots, respectively. Only a little change in electric field distribution is observed in the range of wavelengths (500–542 nm) for the T_{Ag} = 0 nm sample. It means that the generated EM wave from the active layer freely propagates without specific absorption and scattering, resulting in no change in the emission spectrum. Meanwhile, the intensity of EM fields in the T_{Ag} = 5 nm sample is low at the incident wavelength of 500 nm, but it increases with the incident wavelength, as shown in Fig. 5c. It means that the Ag nano-dots played a role in the LSPR occurring on the surface of the Ag nano-dots. That is, the EM intensity reduced as the wavelength decreased. The propagation of the EM wave at λ < 514 nm (the peak center of a normal OLED's emission spectrum) is hindered due to a strong LSPR (Fig. S3†), leading to the shift of the emission spectrum towards a higher wavelength (redshifted). Fig. 5d shows the spectra of the normalized output power of the OLEDs as a function of T_{Ag}. As T_{Ag} increased, the EL spectra shifted towards high wavelengths. The maximum of the emission peak increases from 514 to 528 nm as T_{Ag} increased from 0 to 5 nm, the trend of which is in good agreement with the experimental ones (Fig. 5e).

4. Conclusions

With the Ag nano-dots, we achieved the emission color change of OLEDs from 514 (cyan) to 552 (yellow-green) nm as T_{Ag} increased from 0 to 5 nm. This is achieved by controlling the size and spacing of Ag nano-dots, leading to tuning of the wavelength of LSPR absorption and scattering. From the 2D FDTD simulation, we infer that the LSPR induced by Ag nano-dots could change the emission color of OLEDs. The propagation of the EM wave at λ < 514 nm (the peak center of a normal OLED's emission spectrum) is hindered due to a strong LSPR, leading to the shift of the emission spectrum towards a higher wavelength (red-shifted). It is inevitable to degrade the transmittance due to LSPR. The transmittance of photons in glass/ITO/Ag was as small as 50% (T_{Ag} > 3 nm) around 514 nm-wavelength (Fig. S6†). Nevertheless, the power efficiency in the Ag nano-dot embedded device was measured to be 79% (T_{Ag} = 5 nm) in comparison with the glass/ITO one (Fig. 4b). Even though the degradation of luminance could be minimized by adjusting the Ag nano-dot structure, there is still room to improve its performance. In this work, we proposed a novel way of tuning the emission color in OLEDs, which is widely helpful for optoelectric devices with metallic nanostructures.

References

1 P. Matyba, H. Yamaguchi, G. Eda, M. Chhowalla, L. Edman and N. Robinson, *ACS Nano*, 2010, **4**, 637.
2 T. Sekitani, H. Nakajima, H. Maeda, T. Fukushima, T. Aida, K. Hata and T. Someya, *Nat. Mater.*, 2009, **8**, 494.
3 D. Puzzo, M. Helander, P. O'Brien, Z. Wang, N. Soheilnia, N. Kherani and G. Ozin, *Nano Lett.*, 2011, **11**, 1457.
4 G. Schwartz, S. Reineke, T. Rosenow, K. Walzer and K. Leo, *Adv. Funct. Mater.*, 2009, **19**, 1319.
5 S. Kim, H. Kwon, S. Lee, H. Shim, Y. Chun, W. Choi, J. Kwack, D. Han, M. Song, S. Kim, S. Mohammadi, I. Kee and S. Lee, *Adv. Mater.*, 2011, **23**, 3475.
6 U. Giovanella, M. Pasini, C. Freund, C. Botta, W. Porzio and S. Destri, *J. Phys. Chem. C*, 2009, **113**, 2290.
7 S. Chen and H.-S. Kwok, *Org. Electron.*, 2011, **12**, 677.
8 J. Hou, J. Wu, Z. Xie and L. Wang, *Org. Electron.*, 2008, **9**, 959.
9 S.-H. Cho, J. Oh, H. Park, H. Kim, Y. Lee, J.-G. Lee and Y. Do, *Opt. Express*, 2010, **18**, 1099.
10 W. Barnes, A. Dereux and T. Ebbesen, *Nature*, 2003, **424**, 824.
11 E. A. Coronado, E. Encina and F. Stefani, *Nanoscale*, 2011, **3**, 4042.
12 G. Sujit and P. Tarasankar, *Chem. Rev.*, 2007, **107**, 4797.
13 W. Barnes, *Nat. Mater.*, 2004, **3**, 588.
14 W. Koo, S. Jeong, F. Araoka, K. Ishikawa, S. Nishimura, T. Toyooka and H. Takezoe, *Nat. Photonics*, 2010, **4**, 222.
15 S. Tabakman, Z. Chen, H. Casalongue, H. Wang and H. Dai, *Small*, 2011, **7**, 499.
16 C. Yates, I. Samuel, P. Burn, S. Wedge and W. Barnes, *Appl. Phys. Lett.*, 2006, **88**, 161105.
17 J. Vuckovic and M. Scherer, *IEEE J. Quantum Electron.*, 2000, **36**, 1131.
18 I. Gontijo, M. Boroditsky, E. Yablonovitch, S. Keller, U. K. Mishra and S. P. Denbaars, *Phys. Rev. B: Condens. Matter*, 1999, **60**, 11564.
19 K. Okamoto, *Nat. Mater.*, 2004, **3**, 601.
20 Q. Yu, P. Guan, D. Qin, G. Golden and P. Wallace, *Nano Lett.*, 2008, **8**, 1923.
21 M. Jin, H. Wolferen, H. Wormeester, A. Berg and E. Carlen, *Nanoscale*, 2012, **4**, 4712.
22 M. Heo, H. Cho, J. Jung, J. Jeong, S. Park and J. Kim, *Adv. Mater.*, 2011, **23**, 5689.
23 Y. Xiong, R. Long, D. Liu, X. Zhong, C. Wang, Z. Li and Y. Xie, *Nanoscale*, 2012, **4**, 4416.
24 F. Liu and J.-M. Nunzi, *Org. Electron.*, 2012, **13**, 1623.